



Power Electronic Systems  
Laboratory

© 2013 IEEE

Proceedings of the 28th Applied Power Electronics Conference and Exposition (APEC 2013), Long Beach, California, USA,  
March 17-21, 2013

## **Application of the Magnetic Ear for Flux Balancing of a 16kW/20kHz DC-DC Converter Transformer**

G. Ortiz,  
L. Fässler,  
J. W. Kolar,  
O. Apeldoorn

This material is published in order to provide access to research results of the Power Electronic Systems Laboratory / D-ITET / ETH Zurich. Internal or personal use of this material is permitted. However, permission to reprint/republish this material for advertising or promotional purposes or for creating new collective works for resale or redistribution must be obtained from the copyright holder. By choosing to view this document, you agree to all provisions of the copyright laws protecting it.



Eidgenössische Technische Hochschule Zürich  
Swiss Federal Institute of Technology Zurich

# Application of the Magnetic Ear for Flux Balancing of a 160kW/20kHz DC-DC Converter Transformer

G. Ortiz\*, L. Fässler\*, J. W. Kolar\* and O. Apeldoorn\*\*

\*Power Electronic Systems Laboratory, ETH Zurich

\*\*Power Electronics and Medium Voltage Drives, ABB Switzerland AG

Email: ortiz@lem.ee.ethz.ch

**Abstract**—The non-ideal behavior of semiconductor devices used in power electronic circuits exciting a transformer can cause DC voltage components applied to the transformer terminals. This DC voltage in turn generates a DC current and/or DC flux density component only limited by the parasitic resistance of the windings and semiconductors. The biased flux density operation deteriorates the performance of the converter, since the core can be driven into saturation, generating higher currents and hence higher temperatures in the circuit. In order to overcome this problem, the previously reported "Magnetic Ear", a non-invasive flux density transducer concept, is used in this paper. The design, placement and all implementation issues for this flux density transducer are described. For verifying the theoretical considerations, the transducer is used to perform a closed loop control over the DC component of the flux density in the 166kW/20kHz transformer, therefore ensuring its unbiased magnetic flux density operation.

## I. INTRODUCTION

Isolated and/or high step-up DC-DC converters are built with arrangements of semiconductor switches which provide AC excitation to a transformer. Phenomena such as unmatched turn-on/turn-off times, semiconductor forward-voltage drops, gate driving signal delays or pulsating load, among others, can cause differences in the positive and negative volts-seconds applied to the transformer [1–3]. This results in a DC voltage component at the transformer terminals, which causes an undesired DC current and/or DC magnetic flux density component in the transformer core. The relation between this DC voltage and the resulting DC flux density component is described by [4]

$$B_{DC} = \left( \frac{V_{p,DC}}{R_{p,T}} - \frac{V'_{s,DC}}{R'_{s,T}} \right) \cdot \frac{N_p}{l_M} \cdot \mu_0 \bar{\mu}_r, \quad (1)$$

where  $V_{p,DC}$  and  $V'_{s,DC}$  represent the DC voltage components applied from the primary and secondary side in the transformer respectively,  $R_{p,T}$  and  $R'_{s,T}$  represent the winding resistances plus the semiconductors' equivalent on-state resistances of the primary and secondary side switches respectively,  $l_M$  is the length of the magnetic path,  $N_p$  is the number of turns on the primary side,  $\mu_0$  is the permeability of air and  $\bar{\mu}_r$  is the core's relative permeability in the linear region of the core's B-H curve.

Applying this equation to the 166 kW/20 kHz transformer shown in Fig. 1 (details about this transformer are matter of upcoming publications) only 3 mV of DC bias  $V_{p,DC}$  would suffice to generate a 50 mT DC bias in the flux density of the

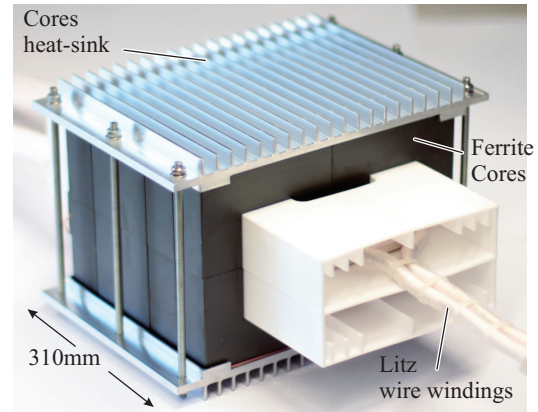


Figure 1: The MEGACube [5] 166 kW/20 kHz transformer to be used as test bench for the described magnetic flux density transducer.

transformer core. This biased magnetic flux density operation results in higher cores losses and potentially in saturation of the transformer core, leading to higher conducted and switched currents which can compromise the converter's efficiency and reliability. For these reasons, an active flux balancing method that ensures an unbiased magnetic flux density operation of the transformer is highly desirable.

Several strategies for ensuring unbiased transformer flux density have been proposed [2, 6–12] whereby a classification and summary of these strategies is presented in [4]. This paper describes the implementation of a closed loop magnetic flux balancing scheme based on the concept proposed in [4], where a novel non-invasive flux density transducer, the "Magnetic Ear" together with the respective control loop was introduced. Details about the transducer concept are presented in **Section II**. In order to successfully implement the flux density transducer on the 166 kW/20 kHz transformer shown in Fig. 1, several practical issues such as transducer geometry, drive circuits and sampling methods are addressed in **Section III**. This leads to the final design of the transducer, whose performance is experimentally validated in **Section IV**.

## II. THE MAGNETIC EAR

The Magnetic Ear flux density transducer's main concept consists on a shared magnetic path between the main core (the actual transformer core) and an auxiliary core represented by the reluctance  $R_m$  in Fig. 2-a), where the trans-

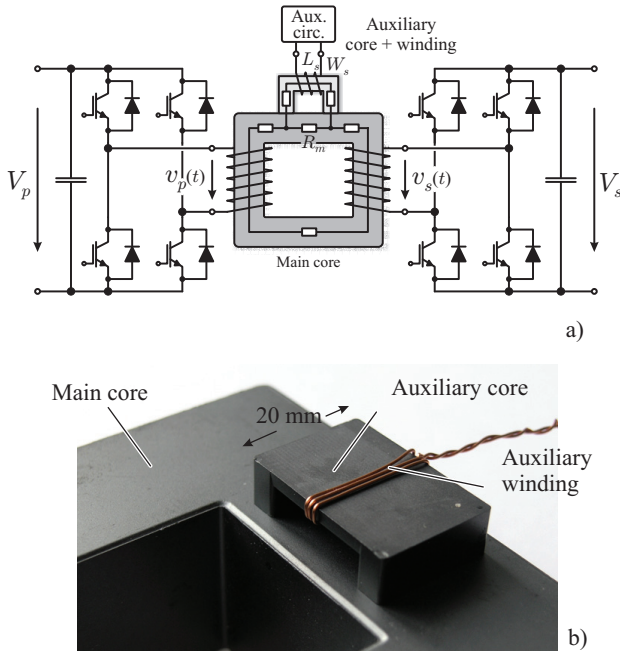


Figure 2: The "Magnetic Ear" main concept: a) Equivalent circuit representation with main core and auxiliary core sharing part of the magnetic path; b) Real implementation of the main core (EPCOS UU93/76/30 N87) and auxiliary core (EPCOS EQ30/8 N87 with removed middle leg) and  $N_{aux} = 3$ .

former serves as link between the primary and secondary side full-bridges, building a dual-active-bridge configuration. This shared reluctance  $R_m$  changes its magnetic properties, namely its relative permeability  $\mu_{r,m}$  as the main core is driven through the B-H loop. This variation results in a change in the inductance  $L_s$  measured from the terminals of the auxiliary core's winding  $W_s$ . This variation in inductance is sensed by an auxiliary drive circuit which extracts the inductance value of the auxiliary core, delivering a signal directly related to the instantaneous magnetization state of the core. The main and auxiliary cores used to test this concept are presented in Fig. 2-b).

The B-H loop of the transformer in Fig. 1 is presented in Fig. 3-a) while the measurement of the inductance for the auxiliary core arrangement shown in Fig. 2-b) is presented in Fig. 3-b) whereby the main and auxiliary cores are built with EPCOS UU93/76/30 N87 and EPCOS EQ30/8 N87 cores respectively. As can be seen, the inductance of the auxiliary core is considerably sensible to the instantaneous magnetization state of the main core, thus the instantaneous value of the auxiliary core's inductance can be used as measure of the magnetization state of the main core. It should be noted that the behavior of the auxiliary core's inductance is depending on the shape of the main core's B-H loop, whereby higher sensitivities are reached if the permeability of the main core continuously changes along the B-H loop. In case the core material is highly linear until saturation is reached, e.g. in gapped cores, this sensitivity is deteriorated and only a change in the inductance can be perceived once the core is driven into saturation. The details and trade-offs

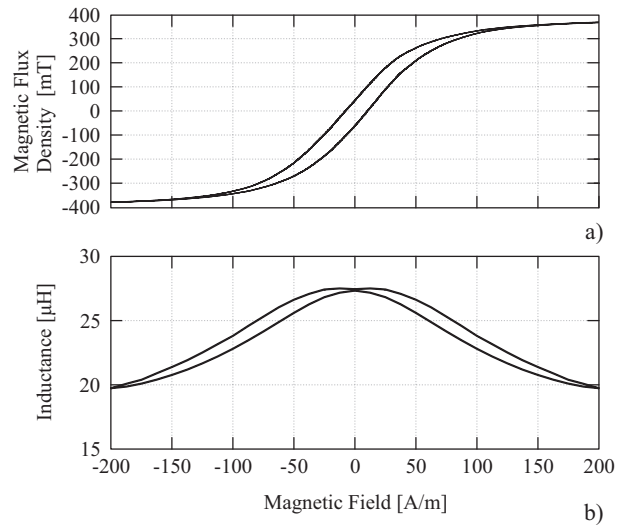


Figure 3: a) B-H loop of the transformer core shown in Fig 1; b) Measured inductance from the auxiliary core's terminals as the main core is driven through the B-H loop.

in the transducer's design, which is ultimately used to control the flux in the main core, will be discussed in the following.

### III. DESIGN, DRIVE CIRCUITS AND SAMPLING METHODS

As mentioned earlier, the Magnetic Ear transducer consists of an auxiliary core with its auxiliary winding and the respective drive circuit used to measure the inductance seen from the auxiliary winding terminals and to convert it to an analog signal. Moreover, in order to implement the feedback loop which performs the flux balancing in the main transformer core, the sampling strategy of the aforementioned signal needs to be studied. As a start, the selection of the appropriate auxiliary core geometry (dimensions) and core material is addressed.

#### A. Auxiliary Core Design

The selection of the auxiliary core's shape and magnetic properties, namely its relative permeability  $\mu_{r,a}$ , will directly affect the sensitivity of the auxiliary inductance  $L_{aux}$  to changes in the main core's permeability  $\mu_{r,m}$ , i.e. changes in the magnetization state of the main core.

In order to analyze the impact of the auxiliary core's geometry and its magnetic properties on the measurement sensitivity, consider the arrangement presented in Fig. 4-a), where a C core is used as auxiliary core. In order to achieve a high sensitivity to changes in the main core's permeability  $\mu_{r,m}$ , the total reluctance of the auxiliary cores' magnetic path must be mainly defined by the shared reluctance  $R_m$  and not by the auxiliary core's reluctance  $R_a$ , i.e.  $R_m \gg R_a$ . These reluctances are defined by:

$$R_a = \frac{l_a}{\mu_0 \mu_{r,a} A_a}, \quad (2)$$

$$R_m = \frac{l_m}{\mu_0 \mu_{r,m} A_m}, \quad (3)$$

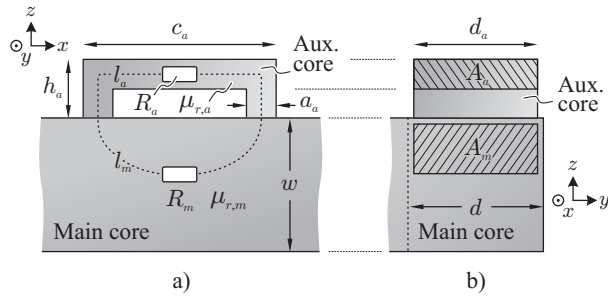


Figure 4: Magnetic flux density transducer, "The Magnetic Ear", geometric definitions.

where  $l_a$ ,  $\mu_{r,a}$  and  $A_a$  are the magnetic path length, relative permeability and cross section of the auxiliary core respectively;  $l_m$ ,  $\mu_{r,m}$  and  $A_m$  are the corresponding values of the shared magnetic path and  $\mu_0$  is the permeability of air. It should be noted that  $A_m$  represents the mean core cross section of the shared magnetic path since this area is not constant along  $l_m$ . Moreover,  $A_m$  is tightly linked with the dimension  $c_a$  of the auxiliary core, as will be shown later in this section.

Considering the definitions from Figs. 4-a) and b), the following observations can be made:

- The height  $h_a$  of the auxiliary core must be as small as possible in order to reduce the length of the auxiliary core's magnetic path  $l_a$  and therefore reduce the reluctance  $R_a$ .
- The width  $a_a$  of the core cross section must be large in order to increase the auxiliary cores's cross section  $A_a$  and therefore reduce reluctance  $R_a$ . For the same reason, the depth of the auxiliary core  $d_a$  must be as close as possible to the depth  $d$  of the main core.
- The permeability  $\mu_{r,a}$  of the auxiliary core must be high in order to reduce the reluctance  $R_a$ .
- The air gap between the auxiliary and the main core must be kept as low as possible since this air gap introduces a constant reluctance that deteriorates the sensitivity of the transducer.
- The number of turns  $N_{aux}$  of the auxiliary core only affects the absolute value of inductance of the auxiliary core but does not affect the sensitivity to changes in the main core's permeability. Therefore low number of turns are suggested in order to reduce the induced voltage in the auxiliary core winding due to the flux in the main core, as will be shown in the next section.

The dimension  $c_a$  of the auxiliary core has a large impact on the transducer's sensitivity. For example, a small  $c_a$  would result in a short magnetic path  $l_m$  and therefore the auxiliary core's inductance would be mainly defined by the auxiliary core's reluctance  $R_a$ . On the other hand, a large  $c_a$  results in a large cross section  $A_m$  of the shared magnetic path and therefore in a small shared reluctance  $R_m$ , thus deteriorating the sensitivity of the transducer. For this reason, the influence of this dimension on the transducer sensitivity was studied by means of FEM simulations. In order to generalize the analysis, a per-unit system is used whereby the width  $w$  of

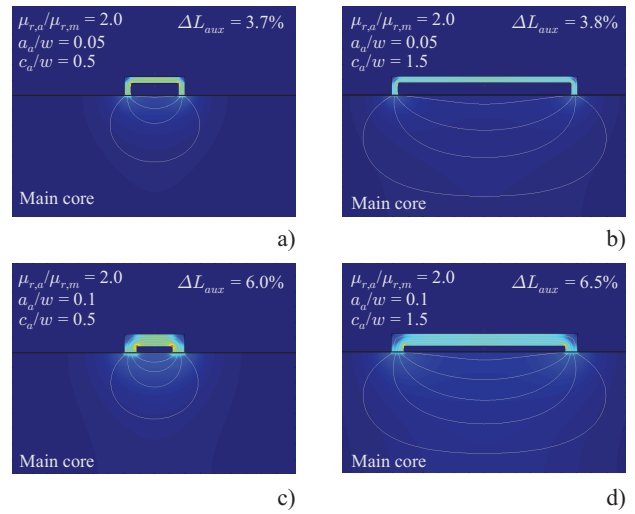


Figure 5: Simulation examples for different auxiliary core geometries. The sensitivities i.e. the changes  $\Delta L_{aux}$  in auxiliary inductance value resulting for various values of  $c_a$  and  $a_a$  (cf. Fig. 4) are presented.

the main core is taken as base dimension while the relative permeability (in non-saturated state)  $\mu_{r,m}$  of the main core is chosen as base permeability value.

As mentioned earlier, the goal is to find the geometry of the auxiliary core which results in the highest sensitivity of the auxiliary core's inductance  $L_{aux}$  to changes in the shared magnetic path's reluctance  $R_m$ . Therefore, the simulation consists of measuring the difference in the auxiliary core's inductance  $\Delta L_{aux}$  when the permeability  $\mu_{r,m}$  of the main core drops by 50% for different values of  $c_a$ . Additionally, the effect of the auxiliary core's permeability  $\mu_{r,a}$  as well as the dimension  $a_a$  in this inductance variation is analyzed since these two parameters were found to have the greatest influence in the transducer's sensitivity.

Fig. 5 shows the magnetic flux density for four exemplary simulations whereby also the respective simulation parameters and resulting inductance variations  $\Delta L_{aux}$  are shown. In Fig. 5-a), a comparatively small value of  $c_a$  was employed, resulting in a short shared magnetic path  $l_m$ . On the other hand Fig. 5-b) shows the resulting flux density distribution for a larger value of  $c_a$ . When compared to Fig. 5-a), the flux lines in this figure show that a larger cross section  $A_m$  is achieved with this value of  $c_a$ , thus no considerable gain in sensitivity is achieved (change in  $\Delta L_{aux}$  from 3.7% to 3.8%) in spite of the larger auxiliary core length  $c_a$ . Similar effects can be seen when comparing Figs. 5-c) and d), where a larger auxiliary core width  $a_a$  was used.

In Figs. 5-c) and d), the results for the same variation in  $c_a$  but with a larger value of  $a_a$  are shown. This increased value of  $a_a$  results in a larger auxiliary inductance variation when compared to Figs. 5-a) and b) due to the larger auxiliary core cross section  $A_a$ , i.e. lower auxiliary core reluctance  $R_a$  while the shared magnetic path's cross section  $A_m$  is not significantly increased, as can be seen from the flux lines in the respective figures.

The performed parametric sweeps are summarized in

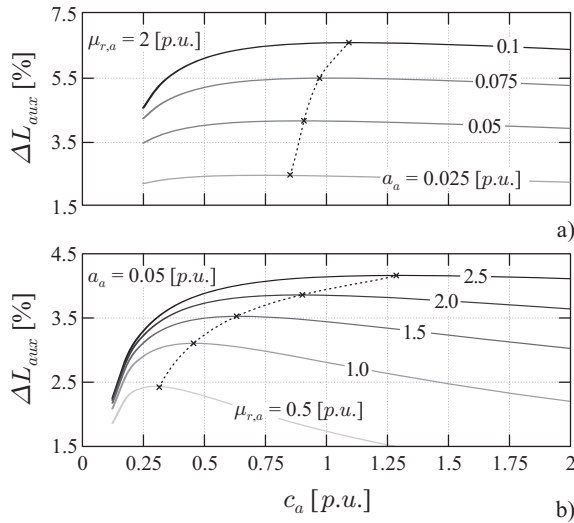


Figure 6: Sensitivity of auxiliary core's inductance variation to different dimensions and permeability as determined by FEM simulations; a) Constant auxiliary core permeability  $\mu_{r,a} = 2.0$ , variable width  $a_a$  and length  $c_a$ ; b) Constant auxiliary core width  $a_a = 0.05$ , variable auxiliary core permeability  $\mu_{r,a}$  and length  $c_a$ .

Fig. 6. In Fig. 6-a), the effect of different auxiliary core widths  $a_a$  for a given auxiliary core permeability ( $\mu_{r,a} = 2.0$ ) is presented. As expected, the variation  $\Delta L_{aux}$  in auxiliary inductance increases with increasing  $a_a$ , as the auxiliary core cross-section is also increased. Moreover, for each value of  $a_a$ , the value of  $c_a$  that maximizes the variation in auxiliary inductance can be found, as shown by the dashed line in Fig. 6-a). However, this optimum is not highly dependent on the core length  $c_a$ , i.e. this dimension and the core width  $a_a$  can be independently selected. As a result, independent of the core length  $c_a$ , the core width  $a_a$  must always be made as large a possible.

The sensitivity of the transducer to variations in the permeability  $\mu_{r,a}$  of the auxiliary core is studied in Fig. 6-b) for different values of auxiliary core width  $c_a$ . As mentioned earlier, a higher permeability of the auxiliary core affects positively the sensitivity of the transducer whereby, the value of  $c_a$  which maximizes the sensitivity can be found for each value of auxiliary core relative permeability, as shown by the dashed line in Fig. 6-b). In this case however, the optimum value of core length  $c_a$  is considerably dependent on the value of relative permeability of the auxiliary core  $\mu_{r,a}$ . For example, if the main core and the auxiliary core possess the same permeability, i.e.  $\mu_{r,a} = 1.0$ , the peak of sensitivity is encountered when the length of the auxiliary core  $c_a$  is 0.45 times the width  $w$  of the main core whereas if the auxiliary core's permeability is 2.5 times that of the main core, the maximum sensitivity is found with an auxiliary core whose length  $c_a$  is 1.3 times the width  $w$  of the main core.

The previous analyses shows that, in order to achieve the highest sensitivity in the transducer, first the relative permeability  $\mu_{r,a}$  of the auxiliary core must be selected as high as possible. Once this property is selected, the length  $c_a$  of the auxiliary core that maximizes the sensitivity for

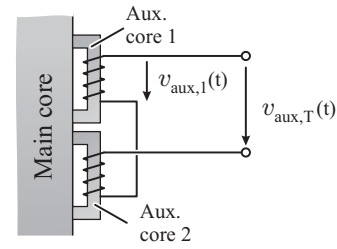


Figure 7: Arrangement of auxiliary cores utilized to reduce the effect of the main core's flux on the auxiliary core inductance measurement.

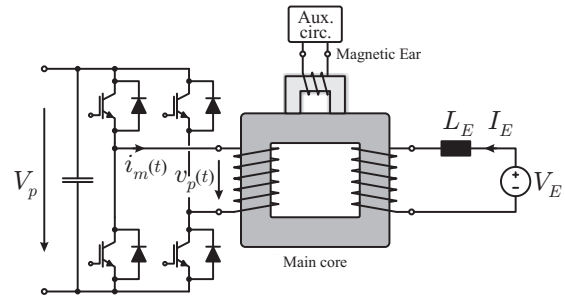


Figure 8: Test circuit consisting on a full bridge driving the transformer's main core, the magnetic flux density transducer and an external circuit utilized to force a DC flux component in the main core.

a given main core width  $w$  can be determined with help of Fig. 6-b).

With the rules for the selection of the auxiliary core dimensions defined, the next step in the implementation of the transducer is the proper placement of the the auxiliary core, which ultimately defines the coupling of the main core's flux with the auxiliary core's winding. This topic is addressed in the following.

### B. Auxiliary Core Placement

The auxiliary core offers a parallel magnetic path for the flux in the main core and therefore an induced voltage in the auxiliary core's winding due to the main flux is encountered. In [4], a placement orthogonal to the main flux direction was proposed, aiming to reduce the effect of this coupling on the measurement of the auxiliary core's inductance. In order to further improve the decoupling from the main core's flux, the arrangement presented in Fig. 7 is proposed. Here, two identical auxiliary cores with windings in opposed orientation are utilized. Nearly identical voltages are induced in the windings of these cores, but due to the opposed orientation, this induced voltages mostly cancel each other out.

In order to test this compensation scheme, consider the test circuit presented in Fig. 8, which is utilized to magnetize the core to nominal flux while the magnetizing current  $i_m$  can be directly measured at the transformer winding. The right hand side circuit is utilized later to force a DC flux component in the core and can be omitted for the testing of the proposed compensation arrangement.

Fig. 9 shows the results of the compensation arrangement

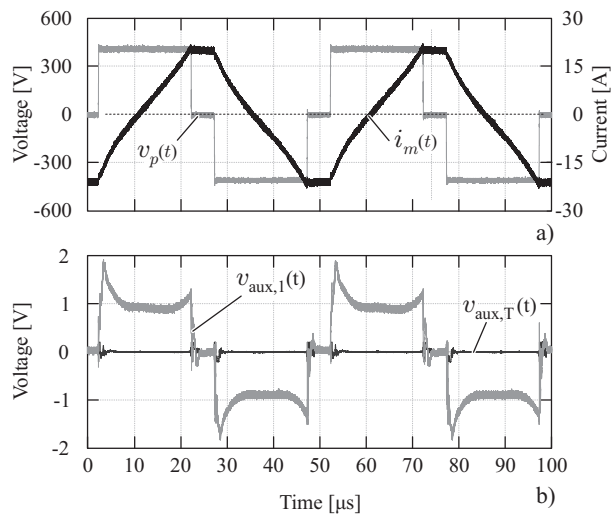


Figure 9: Testing of the compensation arrangement shown in Fig. 7: a) Applied voltage and resulting magnetizing current in transformer of Fig. 1; b) Induced voltage with and without compensation arrangement.

testing. The full-bridge in Fig. 8 supplied with  $V_p = 400$  V, operated with a 20 kHz switching frequency and 40% duty cycle was used to magnetize the transformer in Fig. 1. The resulting primary winding voltage  $v_p(t)$  is shown in Fig. 9-a) together with the corresponding magnetizing current  $i_m(t)$ . The auxiliary cores were arranged as presented in Fig. 7, whereby the voltage  $v_{aux,T}(t)$  induced in the winding of the auxiliary core 1  $v_{aux,1}(t)$  and the compensated signal are depicted in Fig. 9-b). As can be seen, the voltage in a single auxiliary core winding is considerable and would result in a distorted measurement of the auxiliary core's inductance. When compensated, the signal  $v_{aux,T}(t)$  features negligible induced voltage, thus this arrangement can be reliably used in order to extract the auxiliary core's inductance. This last task is performed by the driving circuit of the auxiliary core, as described in the next section.

### C. Drive Circuit

In order to extract the inductance value from the auxiliary core, a constant amplitude high-frequency excitation voltage was used in [4] to drive the auxiliary core, whereby the peak value of the current through the inductor is inversely proportional to its inductance value. This current is later rectified and filtered to generate a low frequency signal directly related to the value of the auxiliary core's inductance and therefore to the magnetization state of the main core.

With the aforementioned driving circuit concept, the filtering stage at the output of the driving circuit defines the bandwidth of the transducer, thus, in order to improve this bandwidth limitation, the driving circuit of Fig. 10-a) is proposed. This circuit consists of two interleaved half bridges phase-shifted by  $90^\circ$  driving each one auxiliary core (each of these cores is then replaced by another pair of cores to compensate for the induced voltage, as shown in Fig. 7) with a switching frequency several times higher than the main core's excitation frequency. Each bridge forces a cur-

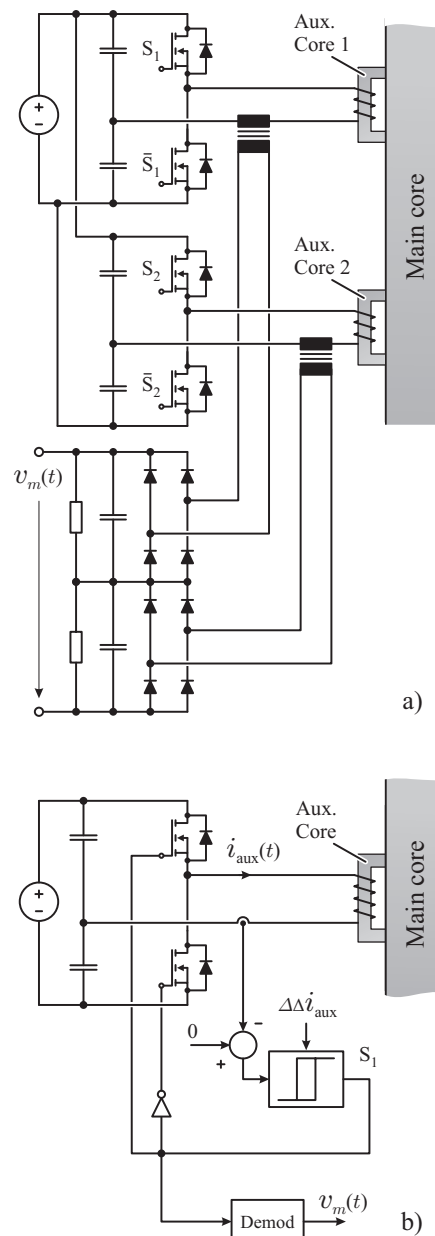


Figure 10: Driver circuits utilized to extract the inductance value of the auxiliary core: a) Interleaved bridges operated at constant frequency and with minimum filtering requirements; b) Constant peak-peak, variable frequency controlled driver. The inductance value is translated into the operating frequency of the bridge.

rent through their corresponding auxiliary cores. Respective current transformers are used to sense this current which, is then rectified by diode bridges. The output diode rectifiers are connected in series, causing the phase shifted currents to compensate the ripple in the output signal  $v_m(t)$ , reducing the amount of required output filter capacitance and therefore increasing the bandwidth of the transducer.

An alternative drive circuit is shown in Fig. 10-b). The main idea of this circuit is to operate the bridge at constant peak-to-peak current by controlling the current with a hysteresis controller whereby the switching frequency of

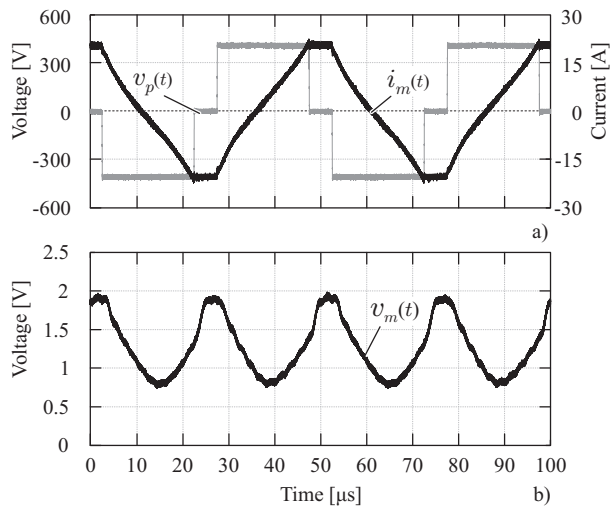


Figure 11: Performance of the magnetic flux density transducer for unbiased operation: a) Excitation voltage  $v_p(t)$  applied by test circuit and resulting magnetizing current  $i_m(t)$ ; b) Output signal of the magnetic flux density transducer  $v_m(t)$ .

the bridge is inversely proportional to the inductance of the auxiliary core. The switching signal at the output of the controller can be later demodulated into an analog signal containing the information about the magnetization state of the main core.

The final transducer, comprising two pairs of auxiliary cores based on EPCOS EQ30/8 cores, was built. This arrangement of cores (one pair for each auxiliary core in Fig. 10-a)) driven by the circuit presented in Fig. 10-a)) was tested with the setup shown in Fig. 8. The resulting output signal  $v_m(t)$  of the transducer is presented in Fig. 11-b). As shown in this figure, the transducer outputs a high signal value when the magnetizing current  $i_m(t)$  reaches a high value, i.e. when the flux in the main core is entering saturation region. On the other hand, the output signal  $v_m(t)$  stays low during the zero crossing of the magnetizing current, i.e. when the magnetic flux in the main core is zero. The slight phase-shift between the peak magnetizing current  $i_m(t)$  and the transducer's output signal  $v_m(t)$  is due to the output filter capacitor of the drive circuit. However, since this signal is sampled only at the end of the freewheeling period, this phase shift does not deteriorate the behavior of the closed loop controller, as described in the last section of this paper.

The aforementioned behavior of the magnetic flux density transducer, comprising the drive circuit from Fig. 10-a), demonstrates the utility of this measurement concept, as the output signal of the transducer is directly related to the magnetization state of the main core. It is now the task of the digital controller to sample the transducer output signal  $v_m(t)$  in order to detect and finally actively correct a biased magnetization state of the main core.

#### D. Sampling Methods

The output signal shown in Fig. 11-b) continuously changes as the magnetization state of the main core is

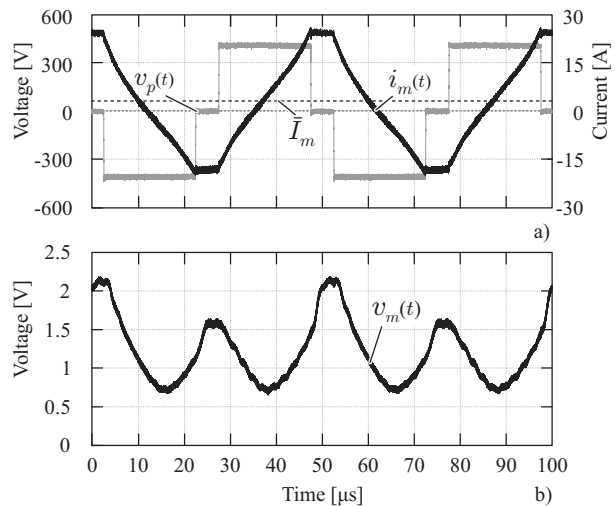


Figure 12: Performance of the magnetic flux density transducer for biased main core operation: a) Excitation voltage  $v_p(t)$  applied by test circuit and resulting magnetizing current  $i_m(t)$  with DC component  $\bar{I}_m$  in the magnetizing current; b) Output signal of the magnetic flux density transducer  $v_m(t)$ .

varying. This signal can be sampled at a high sampling rate, e.g. ten times higher than the frequency of the main core excitation. A lookup table implemented in the digital control platform is utilized in order to translate the signal  $v_m(t)$  into the instantaneous value of the magnetic flux density in the main core.

For the purpose of operating the main core with unbiased flux density, however, sampling the magnetic ear's output signal during the freewheeling states of the full-bridge would suffice to obtain the DC magnetization state of the main core, as explained in [4]. This behavior can be seen from Fig. 12, where a DC component  $\bar{I}_m$  in the magnetizing current, i.e. in the main core's flux density was induced by adjusting the duty cycles on the test bridge (cf. Fig. 12-a)). Fig. 12-b) shows the resulting output signal  $v_m(t)$  from the flux density transducer whereby a clear difference in its peak value can be noticed during two consecutive freewheeling intervals. Due to the biased flux density operation, the output signal  $v_m(t)$  features its peak value at the end of the positive semi-cycle since it's at this point when the main core's permeability is at its minimum, i.e. the auxiliary core's inductance is at its minimum.

The difference between the peak values the output signal at the end of the positive and negative semi-cycles is directly related to the biased magnetization state of the main core. This means that keeping this difference at its minimum is equivalent to minimizing the DC component of main core's magnetic flux density. This strategy is used to actively control the DC component of the magnetic flux density in the core, as will be experimentally shown in the next section.

#### IV. CLOSED LOOP OPERATION

The feedback loop detailed in [4] was implemented on the 166 kW/20 kHz transformer shown in Fig. 1. Two main tests were realized in order to study the dynamic performance

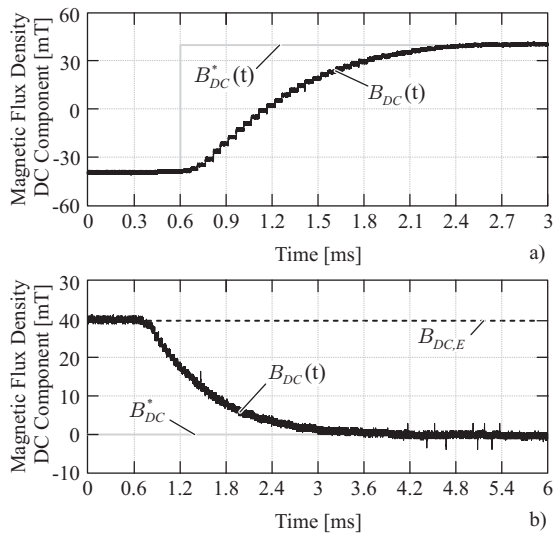


Figure 13: Experimental testing of the feedback compensation scheme: a) Response to step from  $-40$  mT to  $40$  mT in magnetic flux density DC component reference  $B_{DC}^*$ ; b) Response to compensation of externally forced DC flux density component  $B_{DC,E}$ .

of this feedback loop. The first test, shown in Fig. 13-a), consists of a step response from  $-40$  mT to  $40$  mT in the DC flux density component reference  $B_{DC}^*$  applied at  $t=0.6$  ms. As can be seen, the feedback loop is successfully able to regulate within 2 ms the DC component  $B_{DC}$  in the magnetic flux density. Considering the slow dynamics of the potential sources for DC components in the voltage applied to the transformer (e.g. differences in switching times, forward voltage drops and gate driving signal delays), this response time is considered appropriate. Fast modifications in loading conditions can also cause imbalances in the DC flux density component, as described in [8]. However, with modern digital control platforms, this problem can be solved by using the strategy proposed in [11].

The second performed test consists on forcing an external DC flux density component with the external DC source and inductor shown in Fig. 8. By adjusting the current  $I_E$ , the DC flux density component  $B_{DC,E}$  in the main core can be adjusted. This DC component is measured with the Magnetic Ear flux density transducer and used in the feedback loop in order to compensate for it with the main full-bridge. The result of this test is shown in Fig. 13-b). Here, the feedback loop is left off until  $t=0.6$  ms, whereby before this time a forced DC component  $B_{DC,E}=40$  mT can be noticed. As the DC flux density component feedback loop is activated at  $t=0.6$  ms, the DC flux density component  $B_{DC}$  is regulated to zero after 3 ms, achieving an unbiased flux density operation.

These two tests show the effectiveness of the proposed magnetic flux density transducer and its respective drive circuit and feedback scheme, ensuring the unbiased DC flux density operation of the transformer.

## V. CONCLUSION

The "Magnetic Ear" magnetic flux density transducer proposed in [4] was successfully implemented on a real

166 kW/20 kHz transformer, ensuring unbiased DC flux density operation of the transformer. In order to implement this transducer, first a general analysis of the tradeoffs in the selection of the auxiliary core geometry was performed, leading to clear rules which can be utilized to appropriately select the dimensions that best suits the main transformer dimensions. The drive circuit utilized to extract the inductance value of the auxiliary core and therefore to extract the information about the magnetization state of the core were presented. Here, a drive circuit with large bandwidth was utilized, enabling the implementation of a fast feedback loop, which was ultimately utilized to actively control the DC magnetization state of the core, as demonstrated experimentally.

## REFERENCES

- [1] K. O'Meara, "Passive Balancing of Transformer Flux in Power Converters," in *Proc. of the 10th National Solid-State Power Conversion Conference (POWERCON)*, vol. A1, March 1983, pp. 1–11.
- [2] R. Patel, "Detecting Impending Core Saturation in Switched-Mode Power Converters," in *Proc. of the 7th National Solid-State Power Conversion Conference (POWERCON)*, vol. B3, March 1980, pp. 1–11.
- [3] D. Wilson, "A New Pulsewidth Modulation Method Inherently Maintains Output Transformer Flux Balance," in *Proc. of the 8th National Solid-State Power Conversion Conference (POWERCON)*, vol. D1, April 1981, pp. 1–14.
- [4] G. Ortiz, J. Mühlethaler, and J. W. Kolar, "'Magnetic Ear'-based balancing of magnetic flux in high power medium frequency dual active bridge converter transformer cores," in *Proc. of the International Conference on Power Electronics (IPEC)*, May 2011, pp. 1307–1314.
- [5] G. Ortiz, J. Biela, D. Bortis, and K. J. W., "1 Megawatt, 20 kHz, Isolated, Bidirectional 12kV to 1.2kV DC-DC Converter for Renewable Energy Applications," in *Proc. of the International Power Electronics Conference (IPEC)*, June 2010.
- [6] R. Kuttner, "Circuit Techniques for Eliminating Primary Current Unbalance in Push-Pull Power Converters," in *Proc. of the 7th National Solid-State Power Conversion Conference (POWERCON)*, vol. F2, March 1980, pp. 1–9.
- [7] W. M. Polivka, A. Cocconi, and S. Cuk, "Detection of Magnetic Saturation in Switching Converters," in *Proc. of the PCI Conference*, March 1982, pp. 584–597.
- [8] R. Redl, N. Sokal, and C. W. Schaefer, "Transformer Saturation and Unusual System Oscillations in Capacitively Coupled Half-Bridge or Full-Bridge Forward Converters: Causes, Analyses, and Cures," in *Proc. of the Power Electronic Specialists Conference (PESC)*, April 1988, pp. 820–828.
- [9] F. P. Dawson, "DC-DC Converter Interphase Transformer Design Considerations: Volt-Seconds Balancing," *IEEE Transactions on Magnetics*, vol. 26, pp. 2250–2252, September 1990.
- [10] F. Stögerer, J. W. Kolar, and U. Drogenik, "A Novel Concept for Transformer Volt Second Balancing of VIENNA Rectifier III Based on Direct Magnetizing Current Measurement," in *Proc. of the Nordic Workshop on Power and Industrial Electronics Workshop*, June 2000, pp. 134–139.
- [11] J. Claessens and I. Hofsjager, "A flux balancer for phase shift ZVS DC-DC converters under transient conditions," in *Proc. of the Applied Power Electronics Conference and Exposition (APEC)*, March 2006.
- [12] S. Han, I. Munuswamy, and D. Divan, "Preventing Transformer Saturation in Bi-Directional Dual Active Bridge Buck-Boost DC-DC Converters," in *Proc. of the Energy Conversion Congress and Exposition*, September 2010, pp. 1450–1451.